ELSEVIER

Contents lists available at ScienceDirect

Transportation Geotechnics

journal homepage: www.elsevier.com/locate/trgeo



Influence of sleeper geometry on the lateral resistance of bamboo sleepers

Guoqing Jing a, Siqi Liu a, David P. Connolly b, Peyman Aela b,* ©

- ^a School of Civil Engineering, Beijing Jiaotong University, Beijing 100044, China
- b Institute for High Speed Rail and System Integration, School of Civil Engineering, University of Leeds, Leeds LS2 9JT, UK

ARTICLE INFO

Keywords: Lateral resistance Bamboo sleepers Sleeper geometry Ballast Single Tie Push Test, DEM

ABSTRACT

This study investigates the effects of bamboo sleeper geometry on lateral track resistance in ballasted railway systems using the Discrete Element Method (DEM), where ballast is modeled as clumped spherical particles with Hertz-Mindlin contact model for non-linear stiffness. Four sleeper geometries, including traditional rectangular, dumbbell, rectangular-winged, and wedge-winged, were analyzed to evaluate their interaction with ballast under lateral loading. The Single Tie Push Test (STPT) procedure was used to measure lateral resistance, with lateral forces applied via a hydraulic jack. The results highlight that sleeper geometry significantly affects lateral resistance, with optimized designs (rectangular- and wedge-winged) achieving the highest resistance values. For the rectangular-winged sleeper, lateral resistance peaked at 6.85 kN, representing a 54% improvement over the traditional rectangular shape. The study also examines the contributions of ballast components (base, crib, and shoulder) to the overall lateral resistance. Base resistance dominated for all geometries but decreases as the crib and shoulder contributions increase with the non-traditional designs. Normal and tangential force distributions within the ballast were also analyzed, showing enhanced interparticle contact for the winged designs. Overall, the rectangular-winged sleeper was found to provide higher performance compared to the traditional prototype sleeper with respect to meeting track requirements for lateral stability.

Introduction

Lateral track resistance is a crucial factor in ballasted railway tracks to prevent lateral movement caused by train loading and the transmission of thermal forces from rails to the sleepers [1]. The resistance to buckling is governed by the bending stiffness of the rail, the strength of the rail-sleeper fastening, and the ballast-sleeper contact. Considering the rail section is difficult to significantly alter and the lateral resistance of modern fastener systems is rarely exceeded, the interaction between the sleeper and the ballast layer has the greatest promise for improving lateral track resistance. The sleeper base in contact with the ballast bed, the sleeper sides in contact with the crib ballast, and the sleeper ends in contact with the ballast shoulder are the three locations at the sleeperballast interface. Le Pen and Powrie [2] and Ichikawa et al. [3] assert that theoretical soil mechanics principles provide a basis for establishing the limiting value of any resistance component. The sleeper base functions as a shallow foundation susceptible to moment, vertical, and horizontal loads. It was established that during standard railway operations, the predominant mode of failure is more likely to be sliding than bearing. Consequently, the base resistance component can be evaluated

as a function of sliding friction at the ballast-sleeper interface as

$$R_{base} = tan\delta \times W_{sleeper} \tag{1}$$

where $W_{sleeper}$ is the weight of the sleeper (around 1.15 kN for a bamboo sleeper), and δ is the ballast/sleeper friction angle.

The sleeper is prone to movement relative to the crib ballast, allowing the crib resistance along the sleeper sides to be determined as

$$R_{sides} = 2 \times \frac{1}{2} K_0 \gamma_b lh^2 \times tan\delta \tag{2}$$

where γ_b is the ballast unit weight (typically ≈ 17 kN/m³), h' is the effective sleeper height (or depth, typically ≈ 230 mm), and K_0 is the coefficient of lateral earth pressure in the crib.

A straightforward lower bound approach for calculating the sleeper end resistance on the basis of an appropriate passive earth pressure coefficient K_p , taking into account: the sleeper/ballast interface friction, the slope of the ballast shoulder and the inclination (batter) of the sleeper end, gives

E-mail address: p.aela@leeds.ac.uk (P. Aela).

^{*} Corresponding author.

$$R_{end} = \frac{1}{2} K_p \gamma_b w h^2 \tag{3}$$

where, in addition to the symbols already defined, w is the sleeper width. Alternatively, Le Pen and Powrie [2] and Le Pen, Bhandari and Powrie [4] develop an upper-bound mechanism-based approach, for which they present typical results but not a closed-form equation. Fig. 1 shows the contributions of these three components to the total lateral sleeper resistance. It is noteworthy that the sleeper base resistance depends significantly on whether the sleeper is loaded or unloaded, as well as on whether it is well-supported or hanging, which can influence the distribution of forces and overall resistance.

The material and geometry of railway sleepers are two important parameters affecting the lateral track resistance. From the material viewpoint, Aela et al. [5] provided a summary of experimental and numerical studies on the contributions of ballast components (crib, shoulder, and base) to the lateral resistance of various sleeper types under both loaded and unloaded conditions. Results reveal that for unloaded sleepers, the base contributes the highest percentage to lateral resistance, ranging from 40 % to 70 %, while the crib and shoulder contributions vary between 20–45 % and 5–30 %, respectively, depending on the sleeper type.

The geometry of a sleeper is another important parameter that affects the contribution of the crib (Fc), shoulder (Fs), and bottom (Fb) to the overall lateral resistance of the track. Lichtberger [6] described different shapes of steel and concrete sleepers used in railways worldwide. Specialized sleeper designs, such as Y-shaped sleepers [7], X-shaped sleepers [8] and winged sleepers [9] exhibit significantly higher lateral resistance compared to conventional sleepers. For instance, winged sleepers have high lateral resistance, with 55 % coming from the bottom ballast, 28 % from the crib, and 17 % from the shoulder. In contrast, traditional designs like monoblock and standard steel sleepers commonly have reduced lateral resistance at all interfaces. For example, the monoblock sleeper commonly generates approximately 50 % of its resistance from the bottom ballast, 25 % from the crib, and 25 % from the shoulder [10].

Studies on alternatives to conventional steel, concrete, and wooden sleepers have been prompted by the growing need for sustainable materials for railway infrastructure [11–13]. Because of its high tensile strength, compressive capacity, and environmental advantages, bamboo, a rapidly growing, renewable resource, has shown great

promise as a material for railway sleepers [14]. Recent research has emphasized the dynamic properties and mechanical performance of bamboo-plywood composite sleepers (BCSs), indicating their potential as long-lasting and environmentally beneficial substitutes for traditional sleepers. The manufacturing process of the BCS, as described by Jing et al. [15], involved four key steps: mechanical processing, where bamboo was sliced and rolled into structural units; carbonization, using high-temperature treatment to enhance pest and corrosion resistance by decomposing sugars and starches; resin impregnation, applying thermosetting resin to improve hardness, durability, and moisture resistance; and shaping under high pressure in a heated, humid environment, which ensured resin penetration and permanently enhanced the material's mechanical properties.

Wooden sleepers, while cost-effective and lightweight with good vibration-damping properties, suffer from significant limitations including a short lifespan of approximately 12 years when applied untreated [16], high susceptibility to moisture, rot, pests, and fungal decay, leading to frequent maintenance and replacement needs. For instance, around 14 million wooden sleepers are replaced annually in the U.S., contributing to deforestation and environmental strain from chemical preservatives [17,18]. BCSs address these drawbacks by offering enhanced durability through superior resistance to environmental degradation, reduced maintenance requirements due to their pest- and rot-resistant nature, and a lower carbon footprint from bamboo's renewability, while achieving durability levels comparable to concrete sleepers. BCSs have demonstrated ductility similar to wooden sleepers, as well as greater load-bearing capacity, intermediate bending stiffness, and vibration resistance comparable to concrete sleepers. From the environmental aspect, bamboo's accelerated growth (maturing in 3-5 years) facilitates substantial lifecycle CO₂ savings, sequestering 2-3 times more carbon than conventional wood during its growth phase and resulting in 30-50 % lower embodied emissions in production compared to concrete or steel sleepers, while also ensuring net CO2 absorption throughout the product lifecycle [19,20]. Bamboo presents distinct advantages over fiber-reinforced foamed urethane (FFU) sleepers, which, although possessing a lifespan exceeding 50 years and decay resistance, exhibit significantly higher initial CO₂ emissions, up to 2–3 times greater than bamboo due to the synthesis of polyurethane [13]. While FFU can yield long-term savings through recyclability, recycled plastic composites can reduce emissions by 20-40 % through material reuse but may not offer the natural vibration damping of bamboo and necessitate more

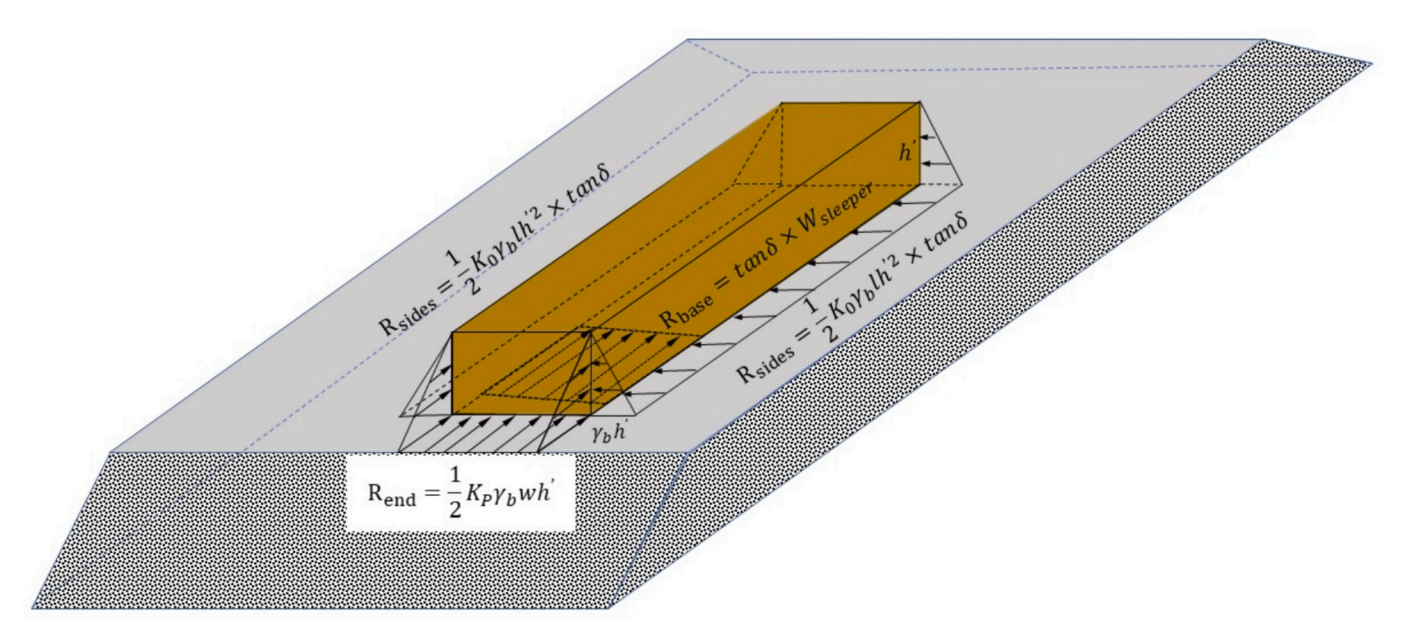


Fig. 1. Force diagram for sleeper-ballast interaction.

energy-intensive processing [21]. In contrast, bamboo's biogenic carbon storage confers superior overall environmental benefits for low-maintenance rail applications. Table 1 provides a comparative overview of key mechanical properties for bamboo, concrete, and wooden sleepers, drawing from recent studies.

Despite these advancements, limited information exists regarding the lateral resistance of bamboo sleepers, particularly concerning the influence of sleeper design on their interaction with ballast.

For the aim of assessing the lateral resistance of an individual sleeper, the Single Tie Push Test is a widely recognized method [24,25]. This test can be performed physically or simulated numerically, typically using the Discrete Element Method (DEM). DEM offers several advantages in simulating sleeper-ballast interactions, including providing microscopic insights into particle-level behaviors such as force chains and contact forces, which help analyze resistance contributions from ballast components like the base, crib, and shoulder; enabling flexible parametric studies by easily varying sleeper geometry, ballast gradation, or loading conditions without physical testing; and allowing validation against experimental setups like the Single Tie Push Test for accurate numerical predictions [26-28]. However, DEM also has notable limitations, such as high computational demands that require substantial processing time, particularly for large-scale 3D models, restricting its use for extensive track simulations; reliance on simplifications like spherical particle shapes or basic contact laws that may not fully capture real-world friction, interlocking, or degradation; challenges in calibration, where tuning micro-parameters such as stiffness and friction coefficients demands extensive experimental data.

To better understand sleeper-ballast interactions, Fig. 2 summarizes the contributions of ballast components in contact with various sleeper types and geometries as investigated by previous researchers [7,8,29-32]. Given that the shape of crib and shoulder ballast can be altered over time due to vibration or loading, it is essential to prioritize the base ballast, as it consistently shows a higher contribution across most sleeper types. Future research should focus on the dynamic effects of loading and vibration on crib and shoulder ballast geometry to determine how these changes influence overall stability and support. Monoblock concrete sleepers exhibit balanced contributions across all components, while winged concrete sleepers show dominant crib ballast engagement (55 %) but lower shoulder contribution. Biblock concrete sleepers similarly rely heavily on crib ballast (57 %), and X-shaped concrete sleepers provide higher side resistance due to their geometry. Innovative designs, like arrowhead-grooved sleepers, help to maximize base resistance, while lightweight fiber-reinforced foamed urethane (FFU) synthetic wood sleepers rely more on shoulder ballast. Y-shaped steel sleepers balance the contributions of base and crib, while U-shaped steel sleepers rely predominantly on base resistance due to their Ushaped design and small side and end contact areas. Changes in sleeper geometry can significantly increase the lateral resistance provided by crib ballast, despite its lack of contribution to the vertical stability or bearing capacity of the track. Additionally, the ballast bed contribution is directly influenced by the sleeper material and weight. For example, plastic sleepers can engage the ballast aggregates more effectively due to their slight deformation, increasing the contact area and enhancing load distribution, whereas concrete sleepers, being stiffer, may not conform as well to the ballast.

Table 1Mechanical characteristics of bamboo, concrete, and wooden sleepers [15,22,23].

Mechanical properties	Bamboo	Concrete	Wooden
Density (g/cm ³)	1.0-1.4	2.4	0.5-0.8
Compressive strength (MPa)	50-80	50	30-50
Tensile strength (MPa)	90-200	4	80-100
Modulus of elasticity (GPa)	15-30	30-60	7–27
Ductility	High	Low (brittle)	High

In this paper, discrete element modeling of STPTs is undertaken to analyze the effect of sleeper geometry on the lateral resistance of BCSs. The unloaded condition is chosen because it represents a critical case in terms of buckling resistance compared to a fully loaded sleeper (recognizing that there can be some slight uplift on a sleeper ahead and behind an approaching train). The absolute and relative contributions of the various sleeper-ballast interfaces (base, crib, and shoulder) to the total lateral resistance, and how these change with the modification of sleeper geometry, are also investigated. The specific objectives of this study are:

- To evaluate the impact of different BCS geometries (rectangular, dumbbell, rectangular-winged, and wedge-winged) on lateral track resistance using DEM simulations of STPTs in an unloaded condition.
- To quantify the absolute and relative contributions of ballast components (base, crib, and shoulder) to the total lateral resistance for each sleeper geometry.
- To analyze how modifications in sleeper geometry alter these ballast contributions, force distributions, and overall track stability.

Methodology

The research is to assess the lateral resistance of bamboo sleepers in a controlled laboratory setting utilizing STPTs. BCSs, regarded as sustainable substitutes for conventional concrete sleepers, were evaluated to assess their lateral stability and performance across different configurations. The manufacturing process of the prototype bamboo sleepers, as described by Jing et al. [15], involved four key steps: mechanical processing, where bamboo was sliced and rolled into structural units; carbonization, using high-temperature treatment to enhance pest and corrosion resistance by decomposing sugars and starches; resin impregnation, applying thermosetting resin to improve hardness, durability, and moisture resistance; and shaping under high pressure in a heated, humid environment, which ensured resin penetration and permanently enhanced the material's mechanical properties.

Prototype BCSs and dumbbell-shaped BCSs were evaluated through STPT experiments to determine their lateral resistance properties (Fig. 3). These two types were chosen because they represent the baseline and an optimized design, respectively, for improving lateral resistance. Other designs, such as rectangular-winged and wedge-winged bamboo sleepers, were analyzed to investigate the effects of geometric modifications on ballast interaction and load distribution via DEM simulations. This choice was primarily due to manufacturing constraints, as producing these designs would require entirely new molds or frames. In contrast, the dumbbell-shaped sleepers were created by modifying the prototype sleeper through cutting the sides, which did not require additional manufacturing frames or molds.

STPT test setup

A track panel with 10 m in length, 3.6 m in width, and 0.3 m in ballast height was constructed using crushed basalt stones. The shoulder width and slope were set to 300 mm and 1:1.75, respectively. The ballast shoulder was kept at the same height as the sleeper for all tests. The large size of the track panel was specifically designed to minimize the influence of ballast confinement and additional resistance forces in the crib ballast zone, ensuring that the measured lateral resistance was representative of actual field conditions. The crushed basalt ballast was prepared following China National Standard TBT 2140 to maintain consistency in particle size distribution, ensuring uniformity across tests. Two Linear Variable Differential Transformers (LVDTs) with 0.001 mm accuracy and a 30 mm range were positioned at the end of the sleeper to measure lateral displacement accurately. The hydraulic jack, used to apply lateral force, was firmly restrained by a custom-built steel frame and positioned directly adjacent to the sleeper to ensure precise force application (Fig. 3). This restraint allowed for the consistent transfer of lateral force to the sleepers without any unintended displacement of the

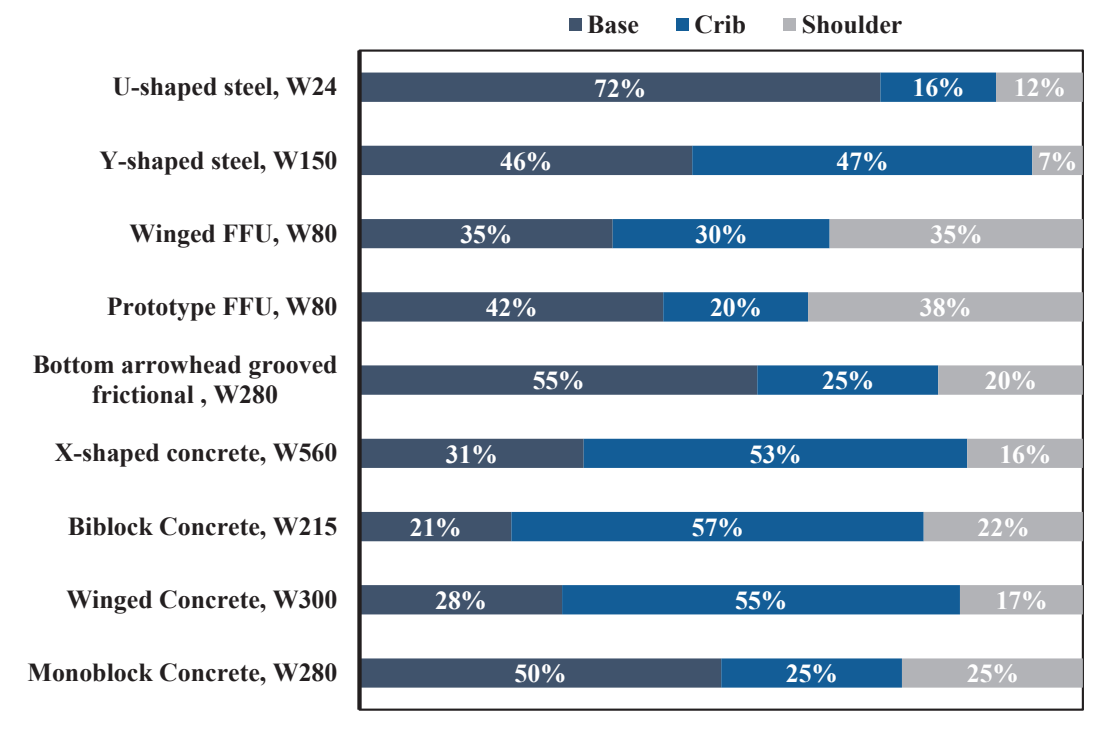
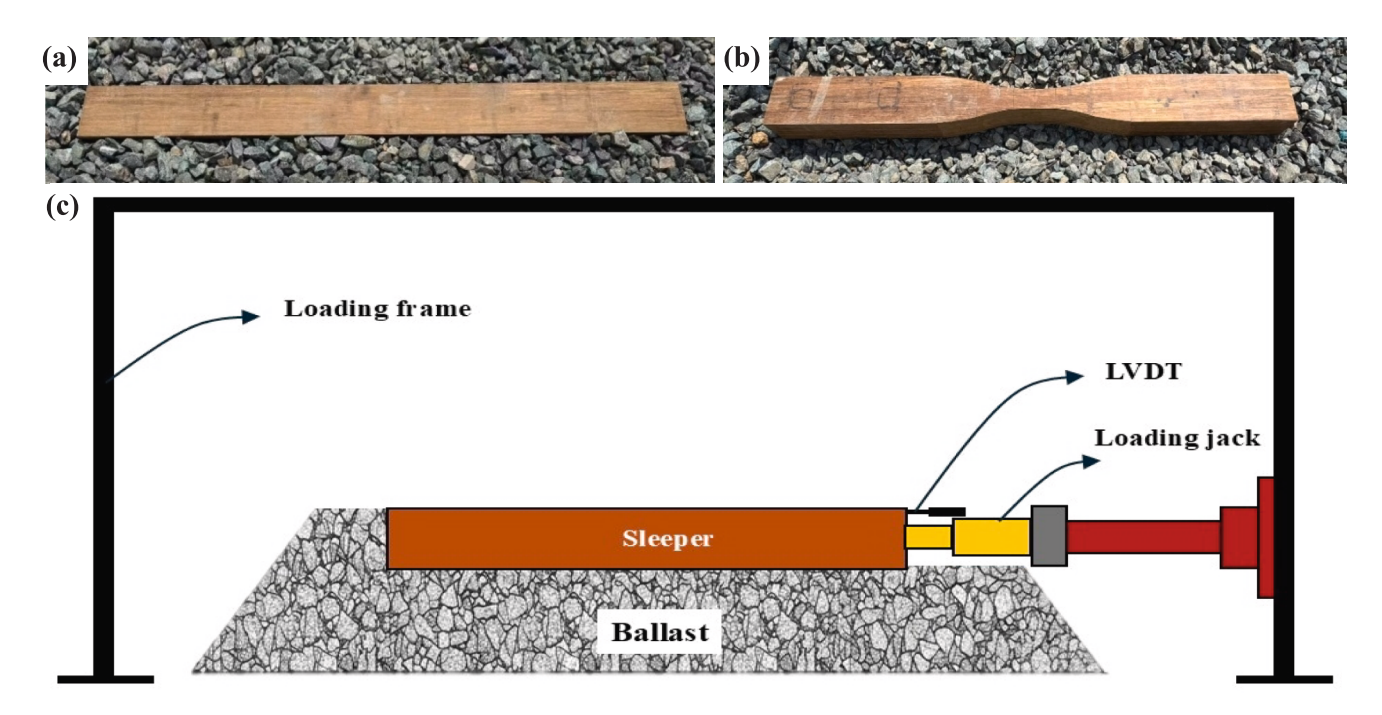


Fig. 2. Contributions of ballast components for various sleepers ("W" denotes the sleeper weight).



 $\textbf{Fig. 3.} \ \, \textbf{(a) Prototype BCS, (b) Dumbbell-shaped BCS, (c) Schematic illustration of the STPT set.} \\$

jack itself. This test setup represents a step ahead of single-sleeper laboratory testing by using a larger ballast bed that incorporates more ballast material and minimizes confinement effects, making it more realistic than lab-scale setups. Although not equivalent to testing on a live railway track, this method provides an improved approximation of field conditions by incorporating a greater volume of ballast.

To record lateral resistance, a data logger (INV3018A) was used, with the resistance recorded at 2 mm displacement, as proposed by the UIC standard [33]. The accuracy and reliability of this setup were validated by conducting repeated trials under identical conditions,

ensuring minimal variation in recorded values and confirming the consistency of results for both sleeper types. Each sleeper was subjected to the same preconditioning process to remove residual effects of previous tests. This involved resetting the ballast configuration and ensuring uniform compaction of the ballast bed for each test.

Modeling of sleepers with different geometries

The sleepers were designed in AutoCAD and exported as STL files, using triangular elements to ensure accurate geometric representation.

For the simulations, the elements were assumed to have an infinite radius of contact with the surrounding particles, thus simplifying the particle interactions. Both the prototype and dumbbell-shaped sleepers were created with dimensions identical to those used in the experimental tests, ensuring consistency between simulation and physical testing (Fig. 4a and b). To further investigate the impact of sleeperballast interaction within the crib zone, two additional sleeper designs were analyzed: rectangular-wing and wedge-wing sleepers (Fig. 4c and d). These designs were specifically chosen to evaluate the influence of different geometrical configurations on ballast behavior, lateral stability and load distribution.

STPT modeling using DEM

DEM is a powerful computational tool for investigating the mechanical behavior of granular materials for understanding both microand macroscopic interactions [34]. For the modeling of ballast and sleepers in this study, DEM is used to simulate the granular system with realistic particle shapes, contact properties, and material interactions. This section outlines the process of generating ballast particles and sleeper models, emphasizing the calibration of parameters and the validation of the model against experiments and standards.

Generation of ballast and sleeper

To simulate ballast particles, the shape, size, particle-particle, and particle-sleeper contact properties were validated using experiments and standards. Ballast particles were modeled as clumps formed from multiple spherical surfaces of different radii and centers of curvature [35]. 10 different 3D-scanned ballast particles comprising clumps of 23-46 pebbles were used as shown in Fig. 5. The formulations of the DEM-based contact model for ballast and sleeper are presented in more detail elsewhere [5,36]. The Hertz-Mindlin contact model was used to represent the non-linear stiffness of the ballast particle contacts. Many of the required parameters could not be measured directly and therefore were determined through calibration, particularly for the material's bulk behavior [36,37]. The required parameters, including interparticle friction, Young's modulus, and Poisson's ratio, were calibrated using tests such as angle of repose, shear, compression, and dynamic ballast box tests [38]. The static (0.85) and rolling (0.15) friction coefficients were calibrated using a systematic technique via angle of repose testing, achieving an error margin of less than 2 %. In order to capture particle,

contact forces and shear behavior, confined compression and direct shear tests were used to determine Young's modulus (25 GPa) and Poisson's ratio (0.25). Ballast box experiments were used to calibrate the restitution coefficient (0.8) under cyclic loads; however, static STPTs are not greatly affected by this parameter. On the other hand, BCSs are represented as non-deformable, high-resolution 3D CAD-derived elements in STL format, that define their geometry with precise surface facets. These meshes are assigned material properties such as density, friction coefficients, and Young's modulus, and are integrated into the simulation as rigid bodies to interact with particle assemblies. The contact between sleeper geometry and ballast particles is handled using Hertz-Mindlin contact model, with adjustments for surface interactions, enabling accurate simulation of force transmission and displacement. The sleeper-ballast friction coefficient was set equal to the value of wooden sleepers in contact with ballast, as reported in [39]. The material parameters and interaction properties used in the simulations are summarized in Table 2.

Simulation of track panels

Fig. 6 illustrates the stages of DEM simulations for STPTs across various ballast configurations: a pure ballast bed to a fully ballasted track. The DEM simulations were performed using EDEM software on a workstation equipped with an Intel Xeon Gold 6240 processor, 64 GB of RAM, and an NVIDIA A100 GPU for CUDA-accelerated solving; each simulation required approximately 30 h of computation time, varying based on the specific sleeper geometry, and particle count (ranging from 331,294 to 344,083 particles). The validation of the DEM model against experimental STPT results, including detailed comparisons of lateral resistance curves, is presented in Section 4.2.2 to assess the accuracy and reliability of the simulation approach. The simulation of BCS on a pure ballast bed aims to evaluate how variations in friction coefficients affect the relationship between lateral displacement and resistance, which is essential for assessing BCS performance under lateral loads. The simulation process begins with generating a ballast bed within a trapezoidal box. The particle size distribution adheres to TBT 2140 specifications [42], allowing particles to fall freely under gravity to fill the domain uniformly. Compaction is then achieved by applying a servo-controlled top platen to settle the particles, progressively reducing void spaces until reaching a target porosity of approximately 0.38 and a corresponding bulk density of 1653 kg/m³ (Fig. 6a). Bulk density is calculated as the ratio of ballast mass to the volume of a designated measurement domain,

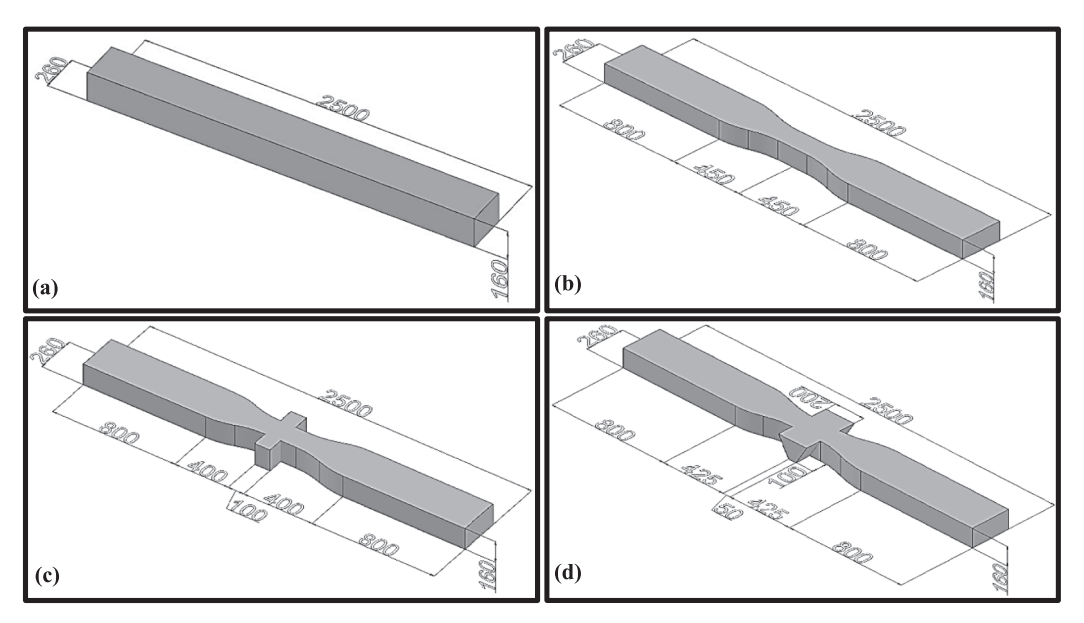


Fig. 4. Dimensions of bamboo sleepers: (a) Prototype, (b) Dumbbell-shaped, (c) Rectangular winged, and (d) Wedge winged sleepers.

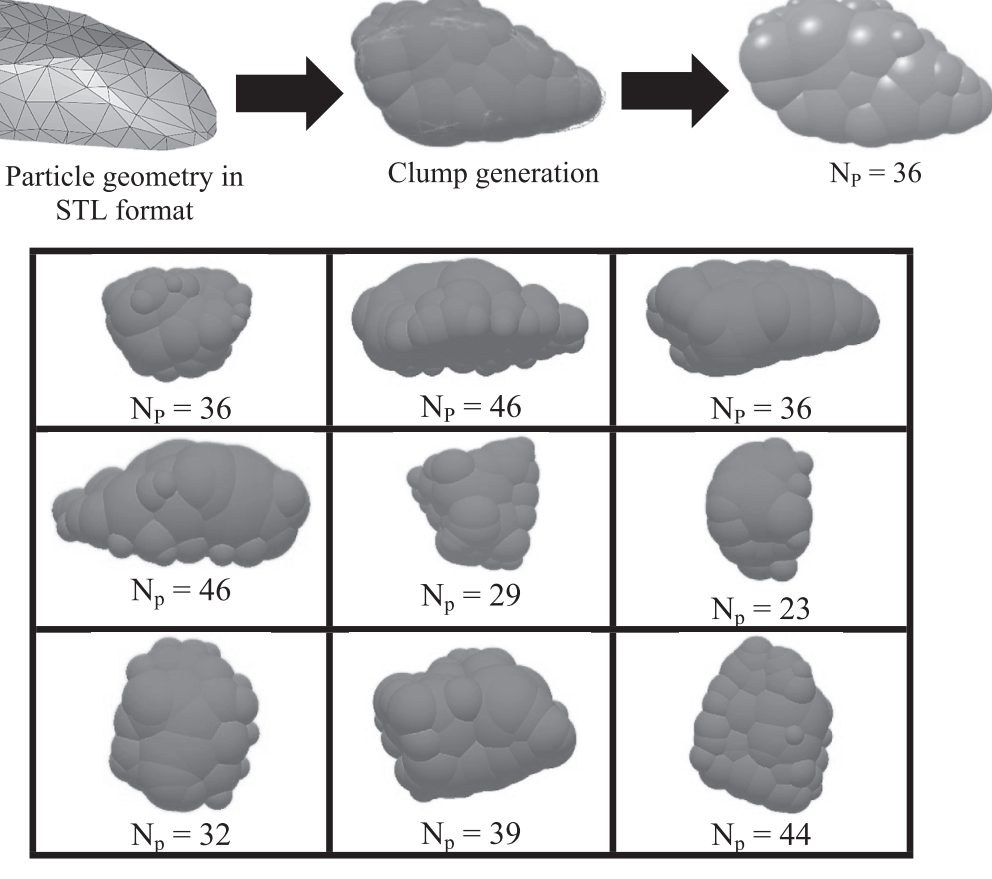


Fig. 5. Ballast particle generation using clumps (Np: number of pebbles per clump).

Table 2
Material properties.

Properties	Ballast [36]	Sleeper [15,40,41]
Material	Basalt	Bamboo
Young's modulus (GPa)	25	15
Poisson's ratio	0.25	0.4
Density (kg/m ³)	2700	1150
Static friction	0.85	0.5
Rolling friction	0.15	1
Coefficient of restitution	0.8	0.8

the under-sleeper zone (highlighted in orange in Fig. 6c), with

dimensions of 600 mm in width, 2900 mm in length, and 300 mm in height. Next, the sleeper is positioned on the ballast bed under gravitational loading. For different BCS types, additional layers of crib and shoulder ballast are incorporated around the sleeper, resulting in a porosity of approximately 0.38 in fully ballasted panels (as detailed in Section 4.2; Fig. 6b). Finally, a lateral force is applied as a linear function of time along the sleeper's length ($F_{\rm x}=200\,{\rm t}$, where t is time in seconds). Unique identifiers are assigned to sleeper components (base, sides, and ends) to record lateral forces and contact points with ballast particles throughout the simulation. Lateral resistance is measured at a sleeper displacement of 2 mm, along with the contributions from each sleeper-ballast interface [33,43]. These contributions were calculated by adding

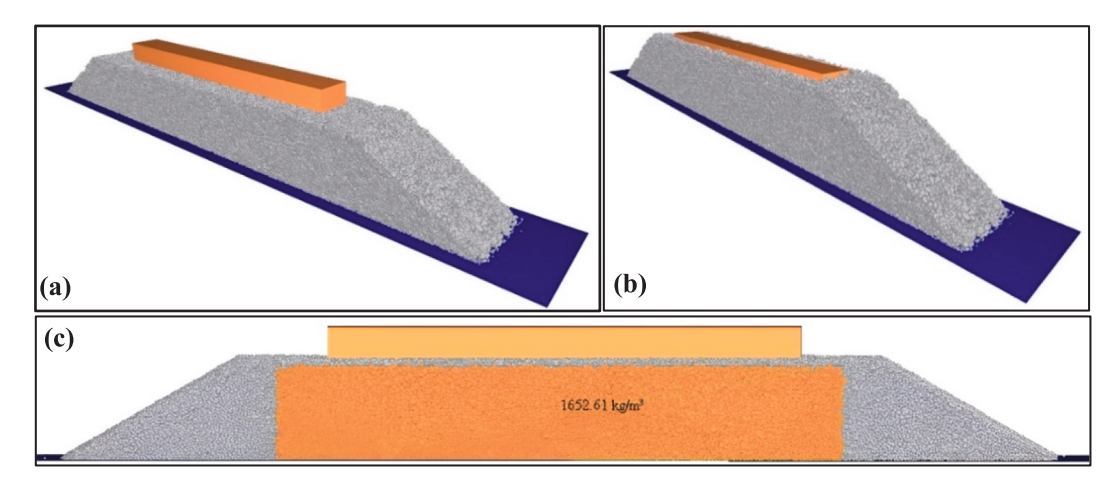


Fig. 6. (a) Sleeper placement on the ballast bed, (b) Fully assembled ballasted track panel, (c) Determination of ballast bulk density.

up the lateral forces on the surface elements of the relevant sleeper faces. Future studies could focus on incorporating advanced measurement techniques, such as Thin Film Pressure Sensors [44], could provide detailed insights into the distribution of stress and force for the sleeper components individually.

Results and discussion

Laboratory test results

The laboratory test results demonstrate the lateral resistance characteristics of three sleepers: concrete, prototype BCS, and dumbbellshaped BCS, under different displacement circumstances. Fig. 7 illustrates lateral resistance (kN) versus displacement (mm) to assess the efficacy of each setup. The configuration of concrete sleepers exhibits the greatest lateral resistance, with a maximum value of 8.05 kN at a displacement of 8.2 mm. This signifies its enhanced load-bearing capacity and rigidity relative to the alternative arrangements. The rectangular BCS has considerable lateral resistance, achieving a maximum value of approximately 5.25 kN at a displacement of 8 mm. This system offers adequate confinement but demonstrates diminished resistance owing to decreased interlocking and rigidity relative to the concrete system. The resistance progressively escalates until a displacement of 3 mm, after which the rate of increase diminishes, signifying a shift from elastic to plastic behavior. The dumbbell-shaped BCS exhibits intermediate performance, with lateral resistance reaching a maximum of 6.67 kN resulting in 27 % enhancement in resistance for the dumbbell configuration relative to the prototype. The higher lateral resistance of dumbbell-shaped BCS demonstrates higher lateral resistance at initial displacements refers to its geometry, which confined the ballast grains that immediately engage a larger volume of ballast in the crib zone through enhanced passive pressure and interlocking mechanisms, mobilizing resistance more effectively compared to the uniform crosssections of concrete sleepers or prototype BCS, where initial resistance relies more on base friction and builds gradually as displacement increases. However, after 1 mm, it shows lower resistance than concrete primarily because the lighter weight and potentially smoother surface of BCS reduce sustained base friction and allow greater ballast rearrangement, dilation, or flow around the narrower middle section at higher displacements, leading to earlier plateauing and reduced ongoing confinement, whereas concrete's greater mass and rougher texture maintain higher resistance through even load distribution and minimized particle shifts.

DEM results

Prior to comparing DEM simulations with experimental STPT results, model verification was conducted following the calibration methodology in Aela et al. [38] for ballast particles. This sequential approach emphasizes tests such as angle of repose for friction, compression and shear tests for particle contact properties. This step confirms the DEM's accuracy in replicating ballast-sleeper interactions, enabling reliable analysis of lateral resistance enhancements.

Calibration of sleeper-ballast coefficient

Calibration of the sleeper-ballast friction coefficient (Fs) is essential for aligning DEM simulations with empirical observations, as it governs the shear resistance at the interface and directly impacts lateral sleeper resistance. In railway engineering, the inter-particle friction coefficient (μ) in ballast typically ranges from 0.4 to 0.8, influenced by factors like particle angularity, surface roughness, degradation, moisture, and fouling [45]. Experimental data from previous studies indicate a friction coefficient rang of 0.665 to 0.872, derived from laboratory tests measuring lateral force required to displace sleepers [46]. It is noteworthy that the friction between wooden or BCS sleepers and ballast is lower than the friction observed with concrete-ballast interfaces. This difference can be attributed to the smoother surface texture and lower density of wooden and bamboo materials compared to concrete, which typically provides a higher coefficient of friction due to its rougher surface and heavier weight. Therefore, the lateral resistance of the prototype BCS was evaluated under friction coefficients of 0.4, 0.5, and 0.6. The results demonstrate that increasing the friction coefficient enhances lateral resistance, underscoring its pivotal role in load transfer mechanisms (Fig. 8a). Specifically, at $F_{\text{S}}=0.6$, the maximum resistance reached approximately 2.55 kN, representing a substantial improvement over the 2.31 kN observed at $F_s = 0.4$, a relative increase of about 10 %. Comparative analysis reveals close alignment between experimental data and simulations when F_s exceeds 0.5, with discrepancies minimized to a 4 % error when the lateral resistance was around 2.4 kN. This convergence validates the calibration process, as lower F_s values (e.g., 0.4) produced underestimations, likely due to insufficient modeling of ballast particle asperity contacts.

Validation of STPTs

The validation of STPT results was performed by simulating the lateral resistance of prototype and dumbbell-shaped sleepers subjected to lateral static loading (Fig. 8). The simulated curves exhibited a high degree of agreement with the experimental results, with an average rootmean-square errors of approximately 5 % across the entire displacement

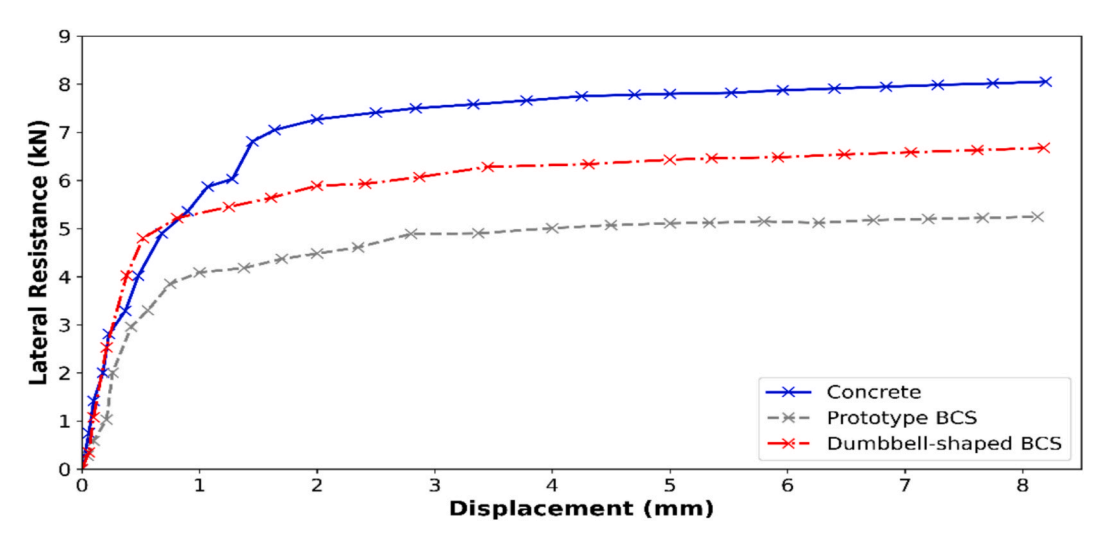


Fig. 7. Laboratory test results.

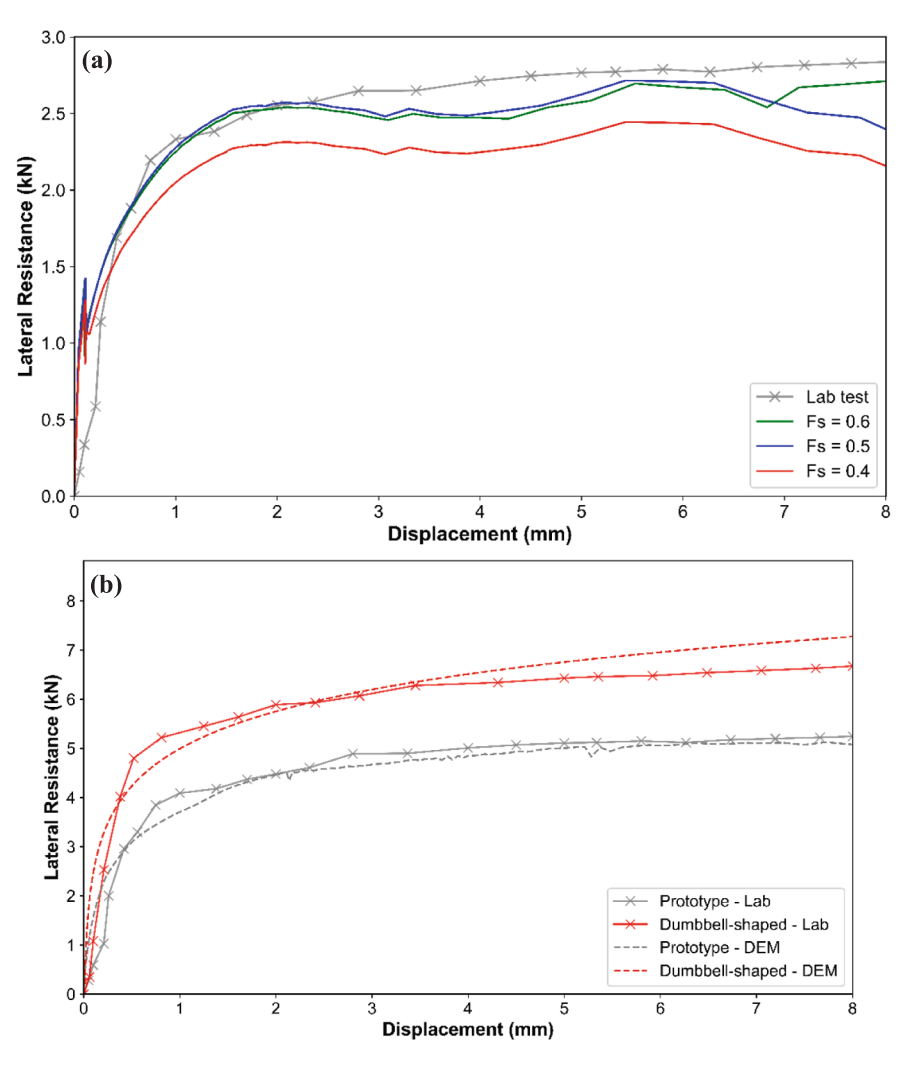


Fig. 8. (a) Force-displacement relationships for the prototype BCS at varying ballast-sleeper friction coefficients, (b) Comparison of DEM and laboratory test results for two BCSs.

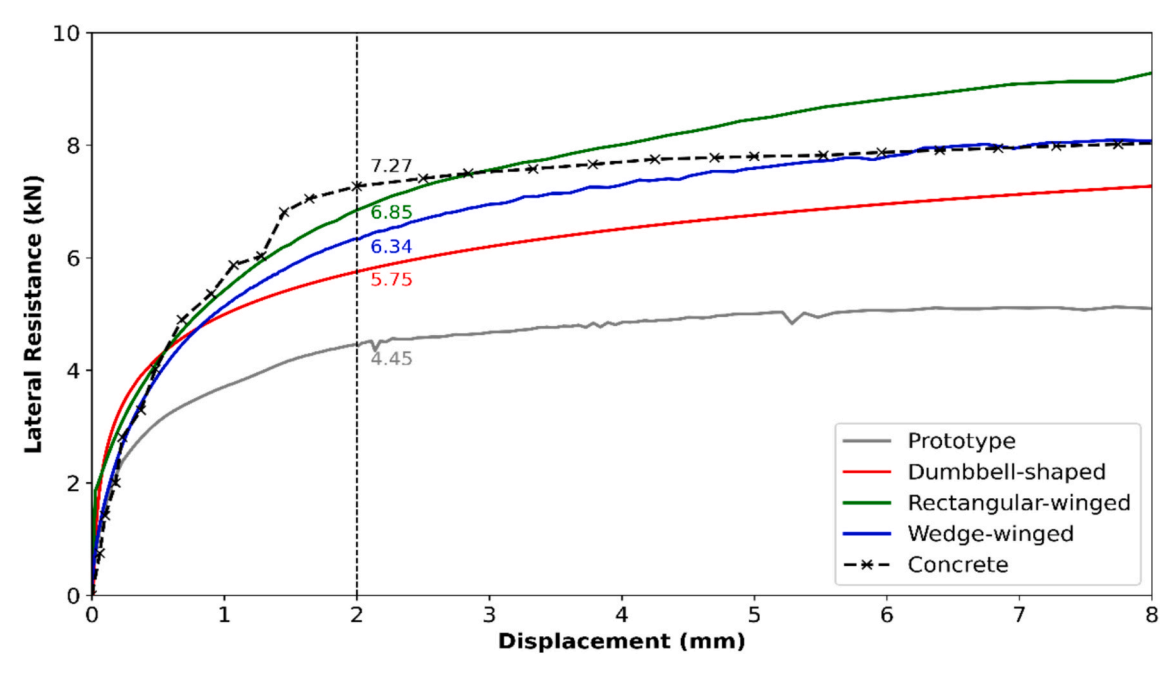


Fig. 9. BCSs total lateral resistance.

range (0–8 mm). In all sleeper arrangements, the first phase (0–2 mm) exhibited a quasi-linear trend, indicative of elastic deformation in the ballast bed. As displacement exceeded 2 mm, the curves entered a clearly nonlinear phase, marked by progressive curvature that signifies plastic deformation and particle rearrangement. Variations in lateral resistance underscore the significant impact of sleeper geometry on ballast bed efficacy. The prototype BCS exhibited an early increase in resistance, stabilizing at around 5 kN after 4 mm of displacement, suggesting minimal engagement of the crib and shoulder ballast. Conversely, the dumbbell-shaped sleeper attained a peak resistance of approximately 7 kN, due to its flared design that facilitates passive pressure mobilization and interlocking with crib ballast particles.

Effect of sleeper geometry on total lateral resistance

To investigate the influence of sleeper geometry on lateral track stability, DEM simulations of STPTs were conducted for four shapes of BCSs, prototype, dumbbell-shaped, wedge-winged, and rectangular-winged, as illustrated in Fig. 4. These geometries were selected to evaluate variations in crib ballast engagement, shear resistance, and load distribution under lateral loading. As depicted in Fig. 9, the lateral resistance-displacement curves for all BCS types exhibit a similar trend between 0 and 0.5 mm, reflecting rapid mobilization of frictional and interlocking forces within the ballast bed, followed by a nonlinear transition and eventual plateau beyond 2–6 mm. This pattern underscores the shift from elastic-dominant to plastic-dominant deformation regimes, with geometry dictating the extent of ballast mobilization.

The prototype sleeper (black curve) exhibited the lowest lateral resistance, stabilizing at approximately 4.45 kN beyond 2 mm, attributable to its minimal crib extensions that restrict passive pressure buildup and ballast interlocking. In contrast, the dumbbell-shaped sleeper (red curve) demonstrated enhanced performance, reaching a plateau of 5.75 kN, a 29 % improvement over the prototype, owing to its curved sides that promote greater crib ballast confinement and passive pressure. The wedge-winged design (blue curve) further surpassed these, achieving 6.34 kN (42 % higher than the prototype), facilitated by its tapered wings that expand the contact area and induce wedge-like penetration into the ballast, enhancing crib ballast-sleeper interlocking.

The rectangular-winged sleeper (green curve) exhibited the superior performance among BCS types, peaking at 6.85 kN and representing a 54 % enhancement relative to the prototype. This superior resistance stems from its broad, uniform wings that maximize interfacial friction and ballast mobilization particularly across the crib zone, effectively distributing lateral forces and mitigating localized deformation. For benchmarking, a conventional concrete sleeper (purple dashed curve) was shown, yielding the highest resistance of 7.27 kN, which the rectangular-winged BCS approaches closely, highlighting the potential of optimized bamboo composites as sustainable alternatives to concrete in terms of lateral stability. Future studies may extend this analysis to variable ballast gradations or long-term cyclic loading to further

validate these geometric benefits.

Contribution of base, crib, and shoulder ballast to the overall lateral resistance

Fig. 10 illustrates the percentage contribution of the sleeper base, crib (sides), and shoulder (ends) ballast to the total lateral resistance for different sleeper geometries. The analysis focuses on understanding how sleeper design influences the distribution of lateral resistance under applied lateral loads. The results show that:

- The sleeper base provides the highest percentage of lateral resistance for the modified shaped BCSs. However, its contribution decreases significantly as sleeper geometry becomes more optimized. For the prototype sleeper, the base accounts for 73 % of the total resistance, while for the wedge-shaped sleeper, it drops to 52 %. This reduction is due to the enhanced role of the crib and shoulder ballast in winged and dumbbell-shaped sleepers.
- The crib ballast contributes moderately to lateral resistance, with its percentage remaining relatively stable across all geometries, ranging from 14 % for the prototype sleeper to 39 % for the rectangularwinged sleeper.
- The shoulder ballast shows a slight increase in contribution for the dumbbell-shaped sleeper, accounting for 16 %, compared to only 13 % for the prototype sleeper. This increase is attributed to the enhanced passive resistance at the sleeper ends, particularly in geometries without winged shapes, and the consequential reduction in the interaction of crib ballast and sleeper sides.

Sleeper-ballast interactions

Fig. 11a shows the number of contacts between ballast particles and sleepers for different sleeper geometries. The results indicate that the number of contacts varies significantly based on the sleeper design. The prototype sleeper records the lowest number of contacts (1,390), followed closely by the dumbbell-shaped sleeper (1,384). The rectangularwinged sleeper shows an increase in contacts (1,680) due to its expanded surface area. The wedge-winged sleeper exhibits the highest number of contacts (2,580), demonstrating superior ballast interaction, which is primarily attributed to its optimized geometry and larger contact surface area. Fig. 11b displays the sleeper-ballast contact forces, categorized into normal and tangential forces, for each sleeper geometry during lateral displacement. The tangential forces dominate the interaction, contributing significantly to the overall lateral resistance. Among the geometries, the rectangular-winged sleeper shows the highest normal and tangential forces, consistently outperforming other designs throughout the displacement range. The rectangular-winged sleeper also demonstrates strong performance, particularly in normal forces, owing to its wide base. The dumbbell-shaped and prototype sleepers show lower normal and tangential forces, with the prototype exhibiting the weakest performance due to its limited contact area. While normal

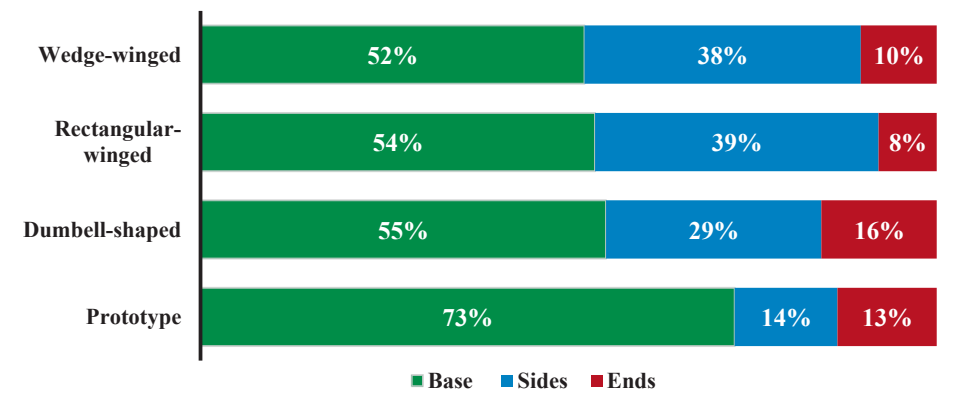


Fig. 10. Percentage of contribution to overall sleeper lateral resistance from the base, crib (side), and shoulder (end).

Number of contacts

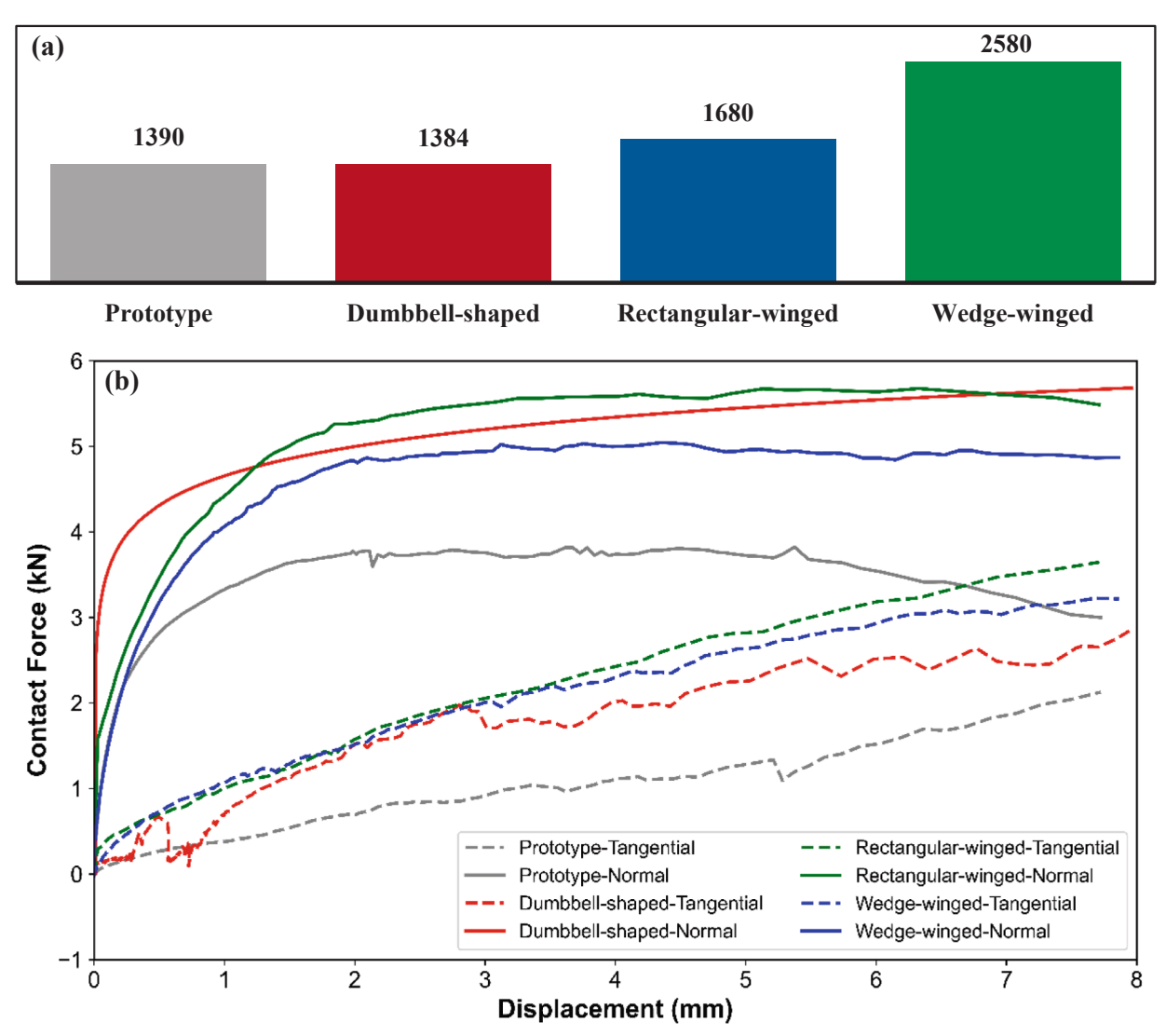


Fig. 11. A) Number of contacts between BCSs and ballast, b) Normal/Tangential force between BCSs and ballast during STPTs.

forces are comparatively smaller across all designs, they contribute meaningfully to the overall resistance. Notably, although the wedge-winged sleeper has the most contacts, the rectangular-winged design yields the highest total resistance due to more effective force mobilization per contact, enhanced normal force distribution and load transfer per contact between sleeper wings and crib ballast, and superior geometric interlocking for passive pressure. Overall, the rectangular-winged sleeper, with its superior contact and force distribution, offers the most efficient design for enhancing lateral resistance and track stability.

Ballast force chain evolution and distribution

Fig. 12 illustrates the normal force distribution within the ballast after 2 mm of sleeper displacement for various sleeper geometries. The forces are represented on a grayscale, where black denotes the maximum normal force and white indicates no force between ballast particles. While normal and tangential forces are comparable in magnitude, the primary contribution to resistance and force distribution arises from normal forces. Therefore, only the normal contact force chains are visualized. The interaction between the crib ballast and sleeper sides at the center zone is significant when the prototype BCS is replaced with the dumbbell-shaped sleepers, resulting in enhanced

stress in these regions. However, the stress distribution across the sleeper base becomes less uniform for rectangular-winged BCS. This reduction in uniformity enhances the overall resistive force compared to other BCSs. At the sleeper ends, larger interparticle forces are primarily observed at the base for prototype and dumbbell-shaped BCSs.

Conclusions

Sleeper lateral resistance is an important parameter contributing to total lateral track resistance. This study demonstrates the influence of bamboo sleeper geometry on the lateral resistance of ballasted railway tracks, with clear benefits from optimized designs. DEM simulations of four sleeper geometries reveal that rectangular-winged and wedgewinged sleepers achieve superior lateral resistance due to enhanced ballast interaction and load distribution. The rectangular-winged sleeper achieved the highest lateral resistance (6.85 kN), outperforming the prototype sleeper (4.45 kN) by 54 %. The validation of STPT results confirms the accuracy of the modeling approach, showing close alignment between the experimental and simulation data. The dumbbell-shaped sleeper demonstrated an approximate 29 % improvement in lateral resistance compared to the prototype, reaching 5.75 kN, attributed to its optimized geometry and improved crib ballast

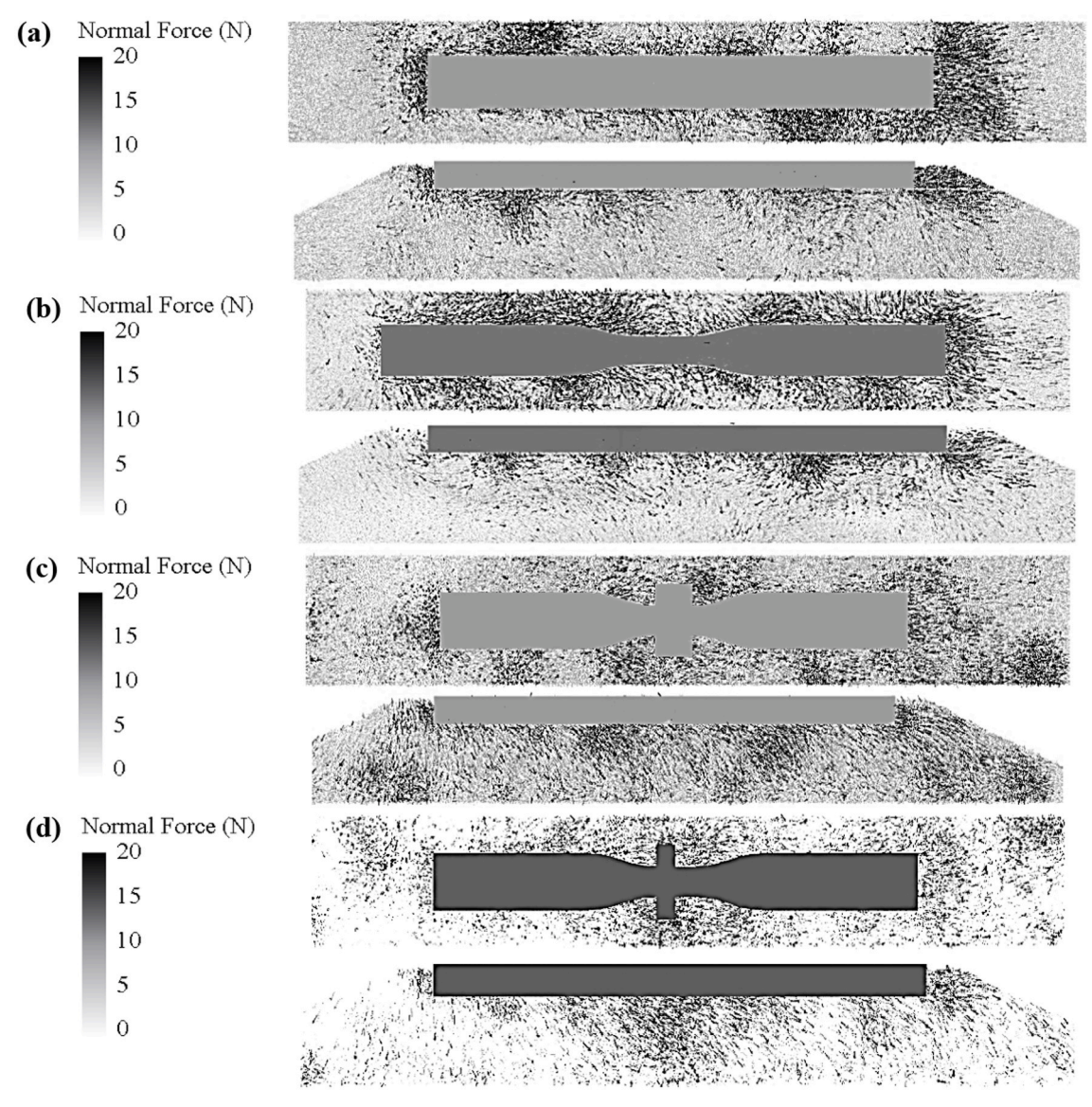


Fig. 12. Normal force distribution: a) Prototype, b) Dumbbell-shaped, c) Wedge-winged, and d) Rectangular-winged sleepers.

interaction. The analysis of ballast components showed that base resistance dominates for all sleeper types but decreases in proportion for optimized designs, as the contributions of crib and shoulder ballast increase. Additionally, the wedge-winged sleeper exhibited the highest number of ballast contacts, underscoring its superior engagement with the ballast.

These findings highlight the potential of bamboo sleepers as sustainable and high-performance alternatives to traditional materials. Optimized sleeper geometries enhance lateral resistance beyond that of traditional rectangular concrete sleepers, indicating bamboo's viability with further design refinements, particularly given that internal reinforcement steel bars in concrete sleepers limit similar shape modifications without manufacturing challenges. Future research should include cyclic loading tests to evaluate long-term durability and ultimate performance under repeated stresses. Also, positive bending strength, fullscale field testing, and long-term durability and vertical stability of BCSs should be further investigated to validate their performance in operational railways. While under-sleeper pads were not included in this study, previous studies indicate that USPs can significantly enhance lateral resistance by improving ballast-sleeper interaction and reducing vibration. Future research should incorporate USPs into bamboo sleeper designs to assess their combined effects. It is acknowledged that the

current investigation was conducted under controlled static laboratory conditions, without accounting for environmental influences (e.g., moisture, temperature variations), full dynamic train loading scenarios, or fatigue factors such as cyclic loading over time. Additionally, long-term performance under these multifaceted conditions can be explored to further validate and expand these results.

CRediT authorship contribution statement

Guoqing Jing: Writing – review & editing, Supervision, Funding acquisition, Conceptualization. **Siqi Liu:** Validation, Methodology, Investigation. **David P. Connolly:** Writing – review & editing, Visualization, Supervision, Formal analysis. **Peyman Aela:** Writing – original draft, Visualization, Software, Project administration.

Declaration of competing interest

The authors declare the following financial interests/personal relationships which may be considered as potential competing interests: Guoqing Jing reports financial support was provided by National Natural Science Foundation of China. If there are other authors, they declare that they have no known competing financial interests or personal

relationships that could have appeared to influence the work reported in this paper.

Acknowledgement

We gratefully acknowledge the National Science Foundation of China (NSFC) [No. 52027813] for their support in the preparation of this paper.

Data availability

Data will be made available on request.

References

- Kish A, Samavedam G. Track buckling prevention: theory, safety concepts, and applications, John A. Volpe National Transportation Systems Center (US); 2013.
- [2] Le Pen LM, Powrie W. Contribution of base, crib, and shoulder ballast to the lateral sliding resistance of railway track: a geotechnical perspective. Proc Instit Mech Eng F: J Rail Rapid Transit 2011;225(2):113–28. https://doi.org/10.1177/ 0954409710397094
- [3] Ichikawa T, Hayano K, Nakamura T, Momoya Y, Koike Y. Prediction of lateral resistance of ballasted tracks based on limiting equilibrium methods. J Japan Soc Civil Eng, Ser E1 (Pavem Eng) 2015;70:I_71-I_77. https://doi.org/10.2208/ isceine.70.1.71.
- [4] Le Pen L, Bhandari AR, Powrie W. Sleeper end resistance of ballasted railway tracks. J Geotech Geoenviron Eng 2014;140(5):04014004.
- [5] Aela P, Zong L, Powrie W, Jing G. Influence of ballast shoulder width and track superelevation on the lateral resistance of a monoblock sleeper using discrete element method. Transp Geotech 2023;42:101040. https://doi.org/10.1016/j. trgep.2023.101040.
- [6] Lichtberger B. Track compendium, PMC Media House, ISBN 39624521412011.
- [7] Aela P, Zong L, Siahkouhi M, Bahari Y, Jing G. Numerical and experimental analysis of lateral resistance of single Y-shaped steel sleeper on ballasted tracks. J Mater Civ Eng 202;34(1):04021414. https://doi.org/10.1061/(ASCE)MT.1943-5533.0004064.
- [8] Chen C, Tang Z-A, Zhang L, Rui R. Comparison of lateral resistance between I-shaped and X-shaped sleepers using finite element and discrete element coupling method. Comput Geotech 2024;165:105889. https://doi.org/10.1016/j.compgeo.2023.105889.
- [9] Jing G, Aela P, Fu H, Yin H. Numerical and experimental analysis of single tie push tests on different shapes of concrete sleepers in ballasted tracks. Proc Instit Mech Eng F: J Rail Rapid Transit 2018:0954409718805274.
- [10] Zhang Z, Xiao H, Wang Y, Fang J, Nadakatti MM, Wang H. Experimental study and discrete element analysis on lateral resistance of windblown sand railway. Transp Geotech 2022;34:100740. https://doi.org/10.1016/j.trgeo.2022.100740.
- [11] Jing G, Siahkouhi M, Riley Edwards J, Dersch MS, Hoult NA. Smart railway sleepers - a review of recent developments, challenges, and future prospects. Construction and Building Materials 271 2021:121533. https://doi.org/10.1016/j. conbuildmat.2020.121533.
- [12] Qahtan AAS, Zeng Z, Ye M, Li P, Li Q, Wang W, et al. An investigative study on the resistance characteristics and vertical stiffness of the novel recycled rubber composite sleeper in a ballasted track structure. Eng Struct 2024;315:118400. https://doi.org/10.1016/j.engstruct.2024.118400.
- [13] Kaewunruen S, Liao P. Sustainability and recyclability of composite materials for railway turnout systems. J Clean Prod 2021;285:124890. https://doi.org/10.1016/ i.jclengo.2020.124890
- [14] He X, Jia W, Dong Y, Siahkouhi M. The application of bamboo in the railway industry: a sustainable solution for track construction. Infrastructures 2023;8(12): 174. https://doi.org/10.3390/infrastructures8120174.
- [15] Jing G, Zhang R, Ngamkhanong C, Tavakol M. Mechanical performance and dynamic characteristics of a novel bamboo-plywood composite railway sleeper. Constr Build Mater 2025;476:141264. https://doi.org/10.1016/j. conbuildmat.2025.141264.
- [16] Quik J, Dekker E, Montforts M. Safety and sustainability analysis of railway sleeper alternatives: application of a novel method for material loops; 2021.
- [17] Goldgaber A. Plastic railroad ties: growing market for alternative materials, SmallcapInsights. com (2009, accessed 5 May 2014) (2009).
- [18] Kaewunruen S, Lopes L, Papaelias M. Georisks in railway systems under climate uncertainties by different types of sleeper/crosstie materials. Lowland Technol Int 2018;20(77–86):1344–9656.

- [19] Xu X, Xu P, Zhu J, Li H, Xiong Z. Bamboo construction materials: Carbon storage and potential to reduce associated CO(2) emissions. Sci Total Environ 2022;814: 152697. https://doi.org/10.1016/j.scitotenv.2021.152697.
- [20] Hinkle H, McGinley M, Hargett T, Dascher S, Carbon farming with timber bamboo: a superior sequestration system compared to wood; 2019. https://www.bamcore. com/_files/ugd/77318d_568cbad9ac2e443e87d69011ce5f48b2.pdf?index=true.
- [21] Luomala H, Halme R, Jönkkäri I. Reducing the carbon footprint of railway sleepers using recycled plastics. Front Sustainability 2024;5–2024. https://doi.org/ 10.3389/frsus.2024.1460159.
- [22] Wang Z, Wei Y, Jiang J, Zhao K, Zheng K. Comparative study on mechanical behavior of bamboo-concrete connections and wood-concrete connections. Front Mater 2020;7–2020. https://doi.org/10.3389/fmats.2020.587580.
- [23] Ticoalu A, Aravinthan T, Karunasena W. An investigation on the stiffness of timber sleepers for the design of fibre composite sleepers, In Proceedings of the 20th Australasian Conference on the Mechanics of Structures and Materials (ACMSM 20): 2008.
- [24] Jeong DY, Samavedam G, Kish A. Determination of track lateral resistance from lateral pull tests. Federal Railroad Administration: United States; 1986.
- [25] Whittle JW, Słodczyk IA, Danks S, Koh LSC, Fletcher DI. Investigating the effect of railway track ballast and bed conditions on the lateral resistance of timber, concrete, steel, and composite sleepers using a novel test methodology. Eng Struct 2025;340:120769. https://doi.org/10.1016/j.engstruct.2025.120769.
- [26] Jia W, Markine V, Carvalho M, Connolly DP, Guo Y. Design of a concept wedgeshaped self-levelling railway sleeper. Constr Build Mater 2023;386:131524. https://doi.org/10.1016/j.conbuildmat.2023.131524.
- [27] Khatibi F, Esmaeili M, Mohammadzadeh S. DEM analysis of railway track lateral resistance. Soils Found 2017;57(4):587–602. https://doi.org/10.1016/j. sandf.2017.04.001.
- [28] Ngamkhanong C, Feng B, Tutumluer E, Hashash YMA, Kaewunruen S. Evaluation of lateral stability of railway tracks due to ballast degradation. Constr Build Mater 2021;278:122342. https://doi.org/10.1016/j.conbuildmat.2021.122342.
- [29] Xiao Y, Shen Z, Tan P, Hua W, Wang M, Jitsangiam P. Evaluating enhancement effect of bottom groove shape on lateral resistance of frictional sleepers in ballasted railway track via hybrid DEM-FDM approach. Constr Build Mater 2024;436: 136755. https://doi.org/10.1016/j.conbuildmat.2024.136755.
- [30] Jing GQ, Zong L, Ji Y, Aela P. Optimization of FFU synthetic sleeper shape in terms of ballast lateral resistance. Sci Iran 2021;28(6):3046–57. https://doi.org/ 10.24200/sci.2021.56898.4970.
- [31] Jing G, Aela P, Fu H, Esmaeili M. Numerical and experimental analysis of lateral resistance of biblock sleeper on ballasted tracks. Int J Geomech 2020;20(6): 04020051. https://doi.org/10.1061/(ASCE)GM.1943-5622.0001689.
- [32] Jing G, Fu H, Aela P. Lateral displacement of different types of steel sleepers on ballasted track. Constr Build Mater 2018;186:1268–75. https://doi.org/10.1016/j. conbuildmat.2018.07.095.
- [33] UIC, Lateral Track Resistance "LTR", UIC-ETF (2019) 32.
- [34] Lu M, McDOWELL GR. Discrete element modelling of railway ballast under monotonic and cyclic triaxial loading. Géotechnique 2010;60(6):459–67. https:// doi.org/10.1680/geot.2010.60.6.459.
- [35] Harkness J. Potential particles for the modelling of interlocking media in three dimensions. Int J Numer Meth Eng 2009;80(12):1573–94. https://doi.org/ 10.1002/mme.2669.
- [36] Aela P, Zong L, Yin Z-Y, Esmaeili M, Jing G. Calibration method for discrete element modeling of ballast particles. Comput Part Mech 2022. https://doi.org/ 10.1007/s40571-022-00507-4.
- [37] Coetzee C. Calibration of the discrete element method: strategies for spherical and non-spherical particles. Powder Technol 2020;364:851–78. https://doi.org/ 10.1016/j.powtec.2020.01.076.
- [38] Aela P, Zong L, Yin Z-Y, Esmaeili M, Jing G. Calibration method for discrete element modeling of ballast particles. Comput Part Mech 2023;10(3):481–93. https://doi.org/10.1007/s40571-022-00507-4.
- [39] Bakhtiary A, Zakeri JA, Fang HJ, Kasraiee A. An experimental and numerical study on the effect of different types of sleepers on track lateral resistance. Int J Transp Eng 2015;3(1):7–15. https://doi.org/10.22119/ijte.2015.13359.
- [40] Irazábal González J. Numerical modeling of railway ballast using the discrete element method; 2015.
- [41] Yap C, Ming T, Wong KJ, Israr HA. Mechanical properties of bamboo and bamboo composites: a review. J Adv Res Mater Sci 2017;35(7–26):2289–7992.
- [42] T.T. 2140-2008, Railway ballast Ministry of Railways of the People's Republic of China, https://www.chinesestandard.net; 2008.
- [43] Zakeri JA, Lateral resistance of railway track, in: I. Xavier Perpinya (Ed.), Reliability and safety in railway, InTech2012, pp. 357-374. doi: 10.5772/35421.
- [44] Tekscan, Thin-Film Pressure Sensors, 2025. https://www.tekscan.com/.
- [45] Suhr B, Butcher TA, Lewis R, Six K. Friction and wear in railway ballast stone interfaces. Tribol Int 2020;151:106498. https://doi.org/10.1016/j. triboint.2020.106498.
- [46] Irazábal González J, Numerical modelling of railway ballast using the discrete element method; 2015. doi: 10.13140/RG.2.2.20125.31200.